Key Engineering Materials
ISSN: 1662-9795, Vol. 926, pp 1075-1082
doi:10.4028/p-zpdi6h

Submitted: 2021-12-20
Revised: 2022-01-21
Accepted: 2022-02-04
Online: 2022-07-22

Deep-Drawing of Commercially-Pure Niobium Sheet

Kelin Chen[1,a], Minki Kim[1,b], Paul Carriere[2,c], James Penny[2.d], Nanda Gopal Matavalam[2.e], Sergey Kutsaev[2,f] and Yannis P. Korkolis[1,g*]

[1]Dept. of Integrated Systems Engineering, The Ohio State University, Columbus, OH, 43210, USA

[2]RadiaBeam Technologies LLC, Santa Monica, CA, 90404, USA

[a]chen.9903@osu.edu, [b]kmknpc@kaist.ac.kr, [c]carriere@radiabeam.com, [d]jpenney@radiabeam.com, [e]nandagopal@radiabeam.com, [f]kutsaev@radiabeam.com
[g*]korkolis.1@osu.edu

*corresponding author

Keywords: Niobium; plastic anisotropy; hardening; deep-drawing; earing.

Abstract. Pure Niobium is a material of interest for high-energy-physics applications including superconducting accelerators. Cold-rolled sheets of Nb exhibit significant plastic anisotropy. Here we report on the mechanical and forming properties of 99.95% pure, 1.02 mm thin, cold-rolled sheet. Uniaxial tension, biaxial tension and disc compression experiments are performed, the first two at multiple angles to the rolling direction of the sheet. The material is very ductile (uniform elongation ~30%), and exhibits significant plastic anisotropy (e.g., the R-values range from 1.2 in 45° to 2.5 in 90°). The results are used to calibrate the Yld2000-2D anisotropic yield function, with an exponent of 6 as Nb is BCC. They are also used to extract the hardening curve beyond the limit load in uniaxial tension. Deep-drawing experiments are performed using a die of 27.6 mm dia. and a punch of 25.4 mm dia. Blanks of various diameters are used. The successfully drawn cups exhibit significant earing. The experiments are simulated using Abaqus/Standard and shell elements. It is shown that a properly calibrated material model enables the numerical simulations to match the experiments.

Introduction

Commercially-pure Niobium (CP-Nb) can be found in a variety of industrial applications and high-energy physics devices, e.g., superconducting cavities for particle accelerators. The cavities are typically produced by two deep-drawn shells welded together to create a spherical shape. Therefore, the mechanical and deep-drawing behavior of Nb sheets is of particular interest.

The mechanical properties of sheet materials, such as yield, hardening, ductility and anisotropy, play an important role in forming processes. A thorough evaluation of these properties requires well-developed experimental setup and careful analysis. Typical sheet metal characterization experiments involve uniaxial tension tests, cruciform tests, bulge tests, plane-strain tension tests or disc compression tests, and have been often used to establish the hardening and plastic anisotropy of sheet metal [1–7]. For Nb in particular, Zamiri and Pourboghrat [8] conducted a set of uniaxial tension tests and proposed an evolving yield function to capture its anisotropy.

A part that is successfully deep-drawn requires to be free of defects such as wrinkling and tearing. These can be avoided or alleviated through tooling adjustment such as the blankholding force. However, it is quite challenging to prevent earing of the part, which is mainly due to the intrinsic plastic anisotropy of the sheets. Therefore, the study of earing of sheet metal has attracted much attention [2, 9–11].

Here we use uniaxial tension tests, biaxial tension tests and disc compression tests to characterize the material hardening and plastic anisotropy of a commercially-pure Niobium sheet. We model the plastic anisotropy using the Yld2000-2d anisotropic yield function [12], and further explore the forming behavior of the sheet via deep-drawing experiments and their numerical simulations.

Mechanical Characterization Experiments

To characterize the strength, hardening and anisotropy of the sheet, five uniaxial tension coupon specimens were cut along the rolling direction (0º), 22.5º, 45º, 67.5º and transverse directions (90º) of the 1 mm thick sheet. Each tensile specimen was tested on a Universal Testing Machine (Instron 5569). A 3D digital image correlation (DIC) setup was used to capture the deformation of the test section. The nominal stress-strain responses for the 5 specimens are shown in Fig. 1a. It can be seen that the sheet is quite ductile with a uniform elongation of about 25% and a significant post-necking elongation before fracture. Moreover, the yield stress also shows a pronounced variation (about 8%) from the lowest yield stress in the RD to the highest yield stress along 45º direction. This is also shown in Fig. 1b in more detail. For a given plastic work of 20 MJ/m^3, the yield stress (normalized by yield stress in RD) increases and then decreases from RD to TD. The R-value, which is defined as the plastic strain in the width direction over that in the thickness direction, shows an opposite trend, with a minimum of 1.2 along 45º and a maximum of 2.4 in TD. The significant variation of the R-values also indicates the sheet is quite anisotropic in the plastic range.

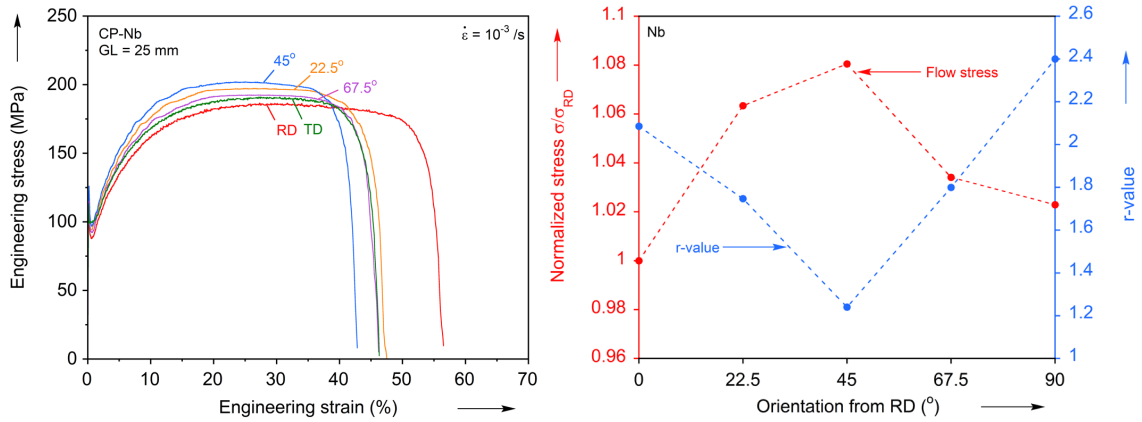

(a) (b)

Figure 1. (a) Engineering stress-strain responses of uniaxial tension specimens along five orientations. (b) The yield stresses (normalized by yield stress in RD) and R-values of the tensile specimens along five orientations.

As a complement to the uniaxial tension tests, three biaxial tension tests with custom designed specimens were also conducted along the RD, 45º and TD. In addition, a disc compression test was conducted, which provided the TD strain over RD strain ratio of about 1.15 under equibiaxial tension, again manifesting a strong anisotropy. Details about the two complementary tests can be found in [13].

Modeling of Plastic Anisotropy

Yield function. Given the strong anisotropy of the material, the Yld2000-2D non-quadratic, anisotropic yield function is adopted to model the anisotropy of the sheet, due to its good flexibility. The equivalent stress in the Yld2000-2D model is expressed as follows:

$$|S_1' - S_2'|^n + |2S_1'' + S_2''|^n + |S_1'' + 2S_2''|^n = 2\sigma_o^n. \quad (1)$$

where S_i' and S_i'', i =1,2,3 are the principal values of the transformed stress tensors $\boldsymbol{S}'$ and $\boldsymbol{S}''$. These are related to the Cauchy stress tensor $\boldsymbol{\sigma}$ through the transformations:

$$\boldsymbol{S}' = \boldsymbol{C}'\boldsymbol{s} = \boldsymbol{C}'\boldsymbol{T}\boldsymbol{\sigma} = \boldsymbol{L}'\boldsymbol{\sigma} \quad \text{and} \quad \boldsymbol{S}'' = \boldsymbol{C}''\boldsymbol{s} = \boldsymbol{C}''\boldsymbol{T}\boldsymbol{\sigma} = \boldsymbol{L}''\boldsymbol{\sigma}. \quad (2)$$

where $\boldsymbol{C}'$, $\boldsymbol{C}''$, $\boldsymbol{T}$, $\boldsymbol{L}'$ and $\boldsymbol{L}''$ are transformation tensors. For plane-stress, the latter two are related to 8 parameters $(\alpha_1, \dots, \alpha_8)$ as:

$$\begin{Bmatrix} L'_{11} \\ L'_{12} \\ L'_{21} \\ L'_{22} \\ L'_{66} \end{Bmatrix} = \begin{bmatrix} 2/3 & 0 & 0 \\ -1/3 & 0 & 0 \\ 0 & -1/3 & 0 \\ 0 & 2/3 & 0 \\ 0 & 0 & 1 \end{bmatrix} \begin{Bmatrix} \alpha_1 \\ \alpha_2 \\ \alpha_7 \end{Bmatrix} \quad \text{and} \quad \begin{Bmatrix} L''_{11} \\ L''_{12} \\ L''_{21} \\ L''_{22} \\ L''_{66} \end{Bmatrix} = \frac{1}{9} \begin{bmatrix} -2 & 2 & 8 & -2 & 0 \\ 1 & -4 & -4 & 4 & 0 \\ 4 & -4 & -4 & 1 & 0 \\ -2 & 3 & 2 & -2 & 0 \\ 0 & 0 & 1 & 0 & 9 \end{bmatrix} \begin{Bmatrix} \alpha_3 \\ \alpha_4 \\ \alpha_5 \\ \alpha_6 \\ \alpha_8 \end{Bmatrix} \tag{3}$$

These 8 parameters introduce the anisotropy, by "scaling" each component of the Cauchy stress tensor differently. Details about the model can be found in [14]. The exponent of 6 is adopted here because the crystal structure of Nb is BCC [15].

The experimental results of five uniaxial tension tests, three biaxial tension tests and a disc compression test are used to calibrate the anisotropy parameters in the model. The stress states and the plastic strain ratios (R-values) at the plastic work density of 20 MJ/m^3 are first extracted and an error function between the experimental and model-predicted values is formed. The anisotropy parameters are then determined by minimizing the error function using Matlab. Details of obtaining the error function can also be found in the Appendix of Chen et al. [16].

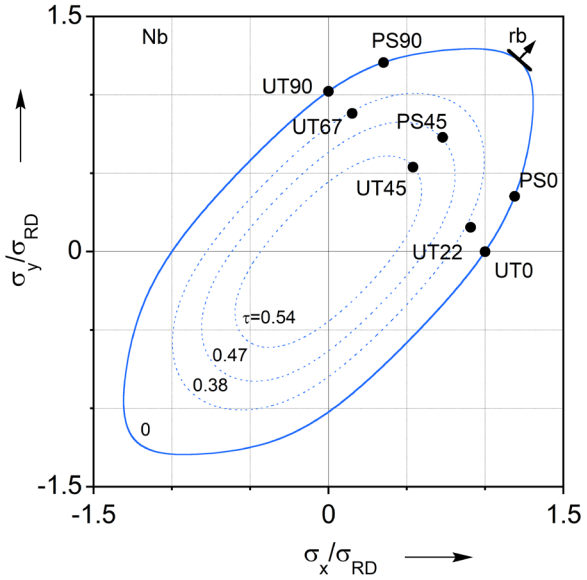

Figure 2. Calibrated yield loci plotted in the RD-TD stress plane and at different shear stress levels and plastic work density of 20MJ/m^3. Included as solid circles are experimental data.

Calibration results. Figure 2 shows the yield loci of calibrated Yld2000-2D in the rolling and transverse stresses plane at different shear stress levels and the chosen plastic work density of 20MJ/m^3 . It can be seen that the experimental data are well captured by the work contours. The yield stress in the neiborhood of equibiaxial tension/compression direction is significantly higher than that in the RD or TD. This could be partially attributed to the very high R-values in RD and TD. The "plane-strain" tension tests also showed some deviation from the ideal zero-transverse strain case, with an trasverse/axial strain ratio of about -1/3, hence in this work they are considered biaxial tension tests, instead (details can be found in [13]). This is also partially because of the high R-value in RD and TD, and the unsuitable geometry used for this material (although the same geometry was highlily statisfactory for other materials [3, 4, 6, 17–19]). Despite that, the biaxial tension tests provide useful biaxial loading information for the anisotropy calibration.

Material Hardening

The uniform true stress-strain response in RD is shown in Fig. 3a as solid dots up to a necking strain of 0.26. The specimen showed a significant amount of stretching after the limit load before the specimen fractured, as shown in Fig. 1a, which implies a strong material hardening effect. Given that the large strain hardening response plays a crucial role in forming simulations, where large deformations are expected, the true stress-strain data beyond the limit load (see Fig. 3a) is inversely identified by comparing the simulated RD axial force-displacement response with the measured one, as shown in Fig. 3b.

The hardening curve was identified by constructing a Finite Element (FE) simulation of the uniaxial tension test. The FE model reproduced the geometry and gripping of the experiment exactly, and was meshed with solid elements in ABAQUS/Standard. An assumed hardening curve provided a force-displacement prediction, which was compared to the experimental one. Then, the input hardening curve was progressively adjusted until the force-displacement prediction matched the experiment exactly. For simplicity, we adopted the von Mises model in the FE simulation. Since we noticed the strong hardening effect in the tensile tests, we first choose a Swift-type extrapolation with a hardening exponent of 0.29 (blue dashed line shown in Fig. 3a). The predicted force-displacement response matches the measured one up to an axial displacement of about 7 mm and then drops abruptly. Then, we switched to the linear extrapolation of the uniform true stress-strain curve (green dashed line shown in Fig. 3a). The extracted force-displacement agrees with the experimental one up to about 8 mm but still falls too early. This implies an even stiffer material hardening curve must be used to match the experimental response. We then adjusted the post-necking stress-strain relationship incrementally in an attempt to match the measured response. The simulated and measured responses match well up to 13 mm, as shown in Fig. 3b. The resulted hardening response is included in Fig. 3a (solid red line), which shows a slight concave-up after the strain of about 0.6. This strong hardening behavior is not common for typical sheet metal such as Steel and Aluminum. A possible explanation is that this material exhibits strong strain-rate sensitivity [13, 20, 21], which is not included in the model adopted, and could effect the results [22]. For example, Peroni and Scapin [23] conducted tensile tests of a Nb sheet at different strain-rates from 10^{-3} /s to 10^{3} /s, and the material responses were found to be strongly rate sensitive. Despite that, the identified curve correctly reproduces the tensile force-displacement response, being the optimal option for the current plasticity model.

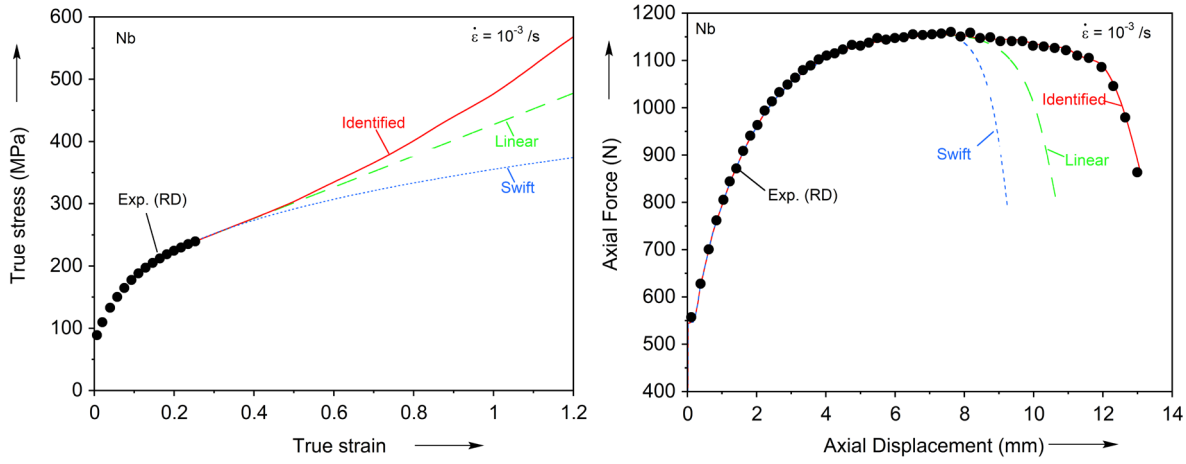

(a) (b)

Figure 3. (a) True stress-strain response in RD up to the onset of necking. Included are extrapolations from Swift hardening, linear hardening and inversely identified hardening. (b) Axial force-displacement of the uniaxial tension test along RD. Included are predictions from the Swift hardening extrapolation, linear extrapolation and identified hardening curve.

Deep-drawing Experiments

Tooling. The sheet forming experiment that is reported here is the deep-drawing with a flat-headed punch. Axisymmetric tooling is used in this study. The punch diameter is 25.4 mm and the die diameter is 27.6 mm. The tooling is integrated in a die-set, as shown in Fig. 4a. The geometry of the tooling is shown in Fig. 4b. Here a spring-loaded blankholder with 4 springs of 11.5 N/mm stiffness each is used. The tooling is made out of AA7075-T6 to avoid possible adhesion between Nb and steel.

The die-set is placed in a Instron 8872 servohydraulic testing machine of 25 kN capacity. The experiments are then performed under displacement control, with the actuator velocity set to 0.1 mm/s. The experiments have been performed with blanks of different diameters, made by wire-EDM. Before each experiment, the blanks and tooling are lubricated with Multidraw PL 61 SE (Zeller+Gmelin). Finally, the blanks are centered in the tooling with a 3D printed centering ring.

Experimental results. Figure 5a shows four fully drawn cups using the deep-drawing tooling shown in Fig. 4. The four blanks have initial diameters of 40, 43.2, 48.3 and 53.4 mm, which correspond to draw ratios of 1.57, 1.7, 1.9 and 2.1, respectively. It can be observed that as the draw ratio increases, the fully drawn cup gets taller, and the earing owing to the significant plastic anisotropy of the material (e.g., Fig. 1b) becomes more obvious. This can be illustrated from the measured minimum and maximum heights of each cup, as presented in Table 1. The difference of the min and max heights (earing height) increases from nearly zero for the drawing ratio of 1.57 to a maximum of 3 mm for the drawing ratio of 2.1.

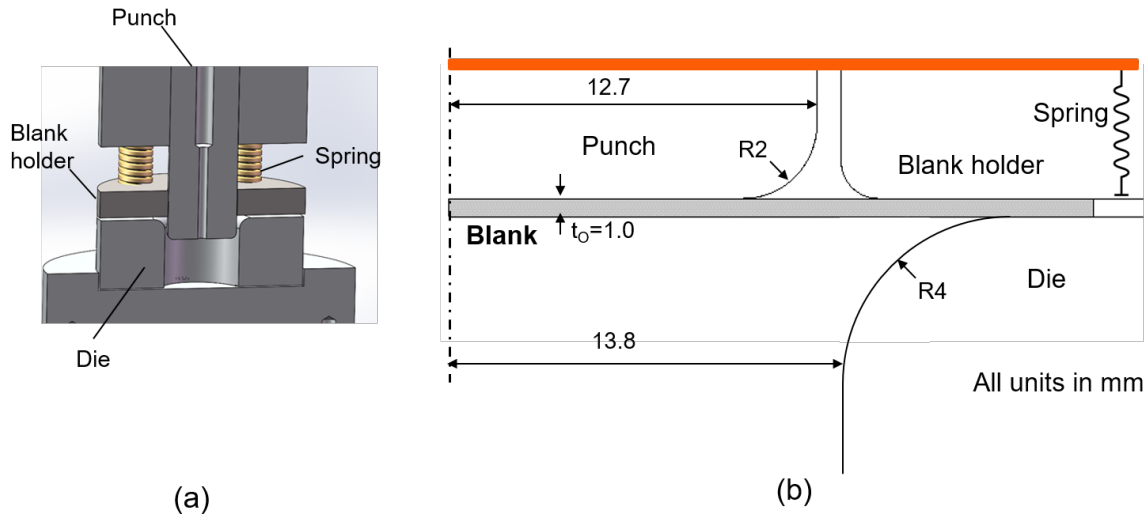

Figure 4. (a) Schematic of the deep-drawing tooling. (b) Dimensions of the tooling.

Table 1. Comparison of the simulated and measured minimum and maximum height of four cups of different drawing ratios. All units in mm.

Drawing Ratio	Min height (exp.)	Max height (exp.)	Min height (FEM)	Max height (FEM)
1.57	11.0 ± 0.6	11.0 ± 0.6	10.2	10.7
1.7	12.6 ± 0.2	13.4 ± 0.3	12.47	13.28
1.9	16.5 ± 0.3	18.0 ± 0.2	16.2	17.8
2.1	21.6 ± 0.4	24.6 ± 0.4	20.25	23.0

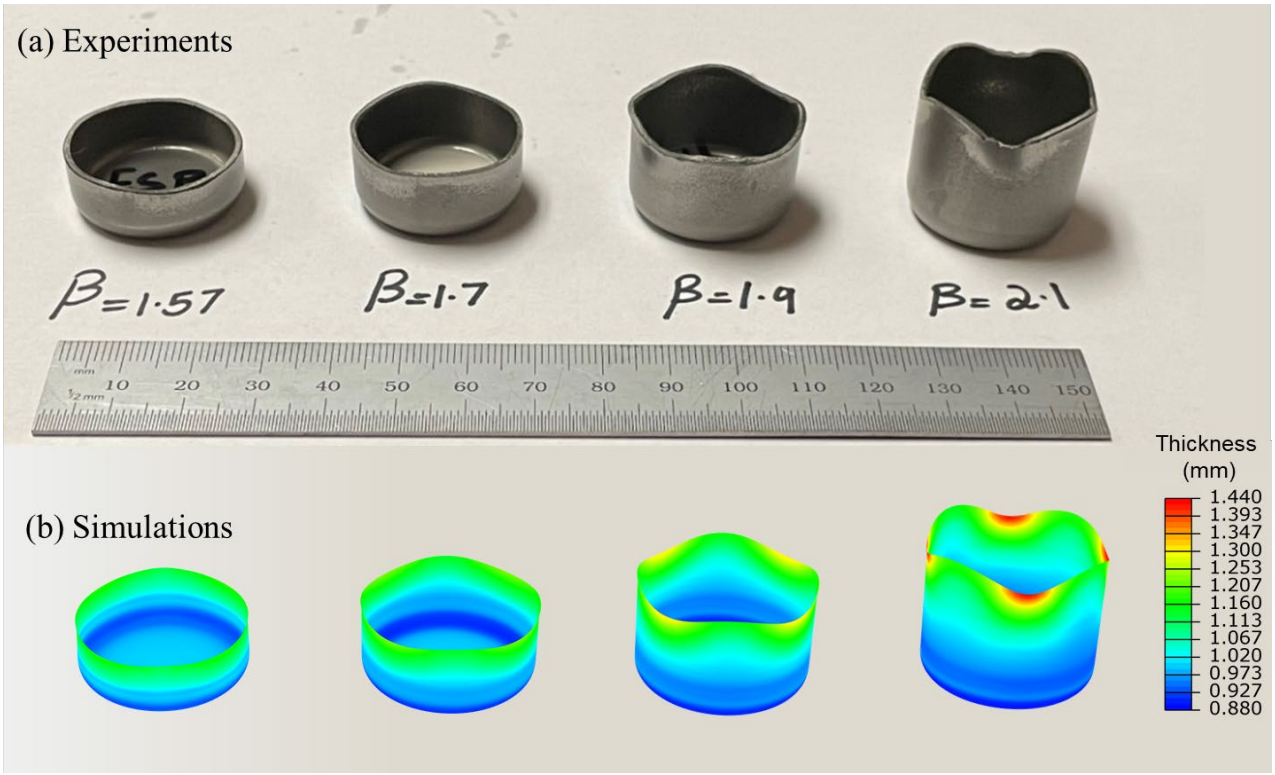

Figure 5. (a) Fully drawn cups with four different drawing ratios. (b) Simulated fully drawn cups that correspond to the drawing ratios shown in (a); the contours indicate the thickness distribution.

Numerical Simulations

FE model. A FE model is developed in ABAQUS/Standard (implicit code) to simulate the deep-drawing process (see Fig. 6). The die, punch and blank-holder are modelled as rigid surfaces. The four springs are modelled with linear spring elements. Due to orthotropic symmetry, only one quarter of the blank is modeled. The Yld2000-2D yield function is introduced in the simulations with a user material subroutine UMAT. To reduce the computational cost of the simulations, the blank is discretized using shell elements (S4R). The mesh of the quarter blank is shown in Fig. 6b, with some key geometric variables also identified (cf. Fig. 4b). During the forming processes, the ram and the punch moved down at the same speed until the process is finished, which leads to a linearly increasing blank holding force as the draw depth increases. Contact between the blank and the tooling is modelled as exponential soft contact with finite sliding. Without a method to directly measure, or indirectly infer, the friction coefficient in the actual deep-drawing processes, the friction coefficient of 0.15 is adopted in the simulations.

Simulation results. Figure 5 compares the simulated and drawn cups with different drawing ratios. It can be seen that the four ears of each cup are well predicted by the FE model. This is because the Yld2000-2D anisotropic yield function is flexible enough to be able to capture the variation of R-value shown in Fig. 1b. Both the average height and earing height of the cups are in good agreements, as quantified in Table 1.

The superimposed contour on the simulated cups represents the thickness distribution. It is noted that the deep-drawing process involves a significant amount of draw-in of the flange, and hence the wall becomes thicker near the outer part of the flange region. It is interesting to note that even though the punch-die clearance is 1.1 mm (see Fig. 4b), the cup wall is predicted to be thicker than that, locally. A certain amount of wall-thinning can be seen in the lower part of the cups, particularly near the punch radius region. Under an excessive blankholding force, e.g., by using stiffer springs, this would lead to tearing at that location.

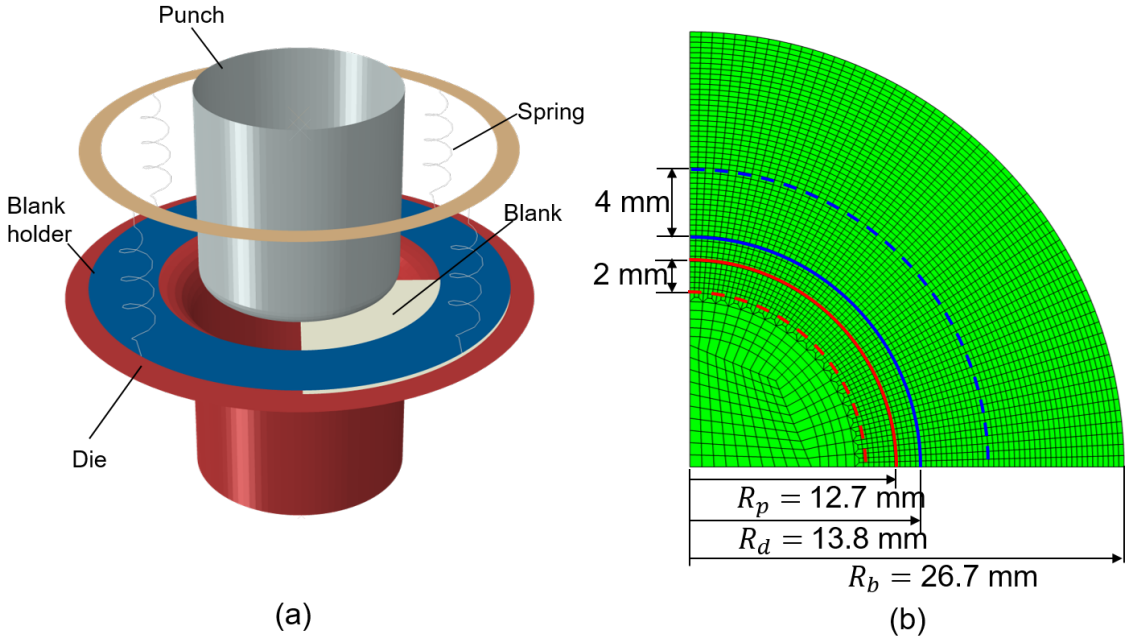

Figure 6. (a) Schematic of the deep-drawing tooling used in the simulations. (b) FE mesh of a quarter blank with some key dimensions of the tooling.

Summary

The plasticity and deep-drawing behavior of a commercial Nb sheet was investigated in this work. The key findings can be summarized as:

- The material shows significant strain hardening and plastic anisotropy.
- The large deformation hardening response is inversely identified from numerical simulations.
- The Yld2000-2D model is capable of capturing the material anisotropy.
- The sufficient formability of this material is demonstrated by successful deep-drawing even at a drawing ratio of 2.1.
- Shell element models provide reliable predictions of the earing behavior.

Acknowledgement

The support of the US Dept. of Energy is acknowledged with thanks. We also thank Pashupati Dhakal and James Spaldin from Jefferson National Laboratory for their help during the course of this work.

References

[1] Tardif N, Kyriakides S (2012) Determination of anisotropy and material hardening for aluminum sheet metal. In: International Journal of Solids and Structures. Pergamon, pp 3496–3506

[2] Tian H, Brownell B, Baral M, Korkolis YP (2017) Earing in cup-drawing of anisotropic Al-6022-T4 sheets. Int J Mater Form 10:329–343. https://doi.org/10.1007/s12289-016-1282-y

[3] Ha J, Coppieters S, Korkolis YP (2020) On the expansion of a circular hole in an orthotropic elastoplastic thin sheet. Int J Mech Sci accepted:

[4] Ha J, Fones J, Kinsey BL, Korkolis YP (2020) Plasticity and formability of annealed, commercially-pure aluminum: Experiments and modeling. Materials (Basel) 13:. https://doi.org/10.3390/ma13194285

[5] Dick CP, Korkolis YP (2015) Anisotropy of thin-walled tubes by a new method of combined tension and shear loading. Int J Plast 71:. https://doi.org/10.1016/j.ijplas.2015.04.006

[6] Baral M, Ha J, Korkolis YP (2019) Plasticity and ductile fracture modeling of an Al–Si–Mg die-cast alloy. Int J Fract. https://doi.org/https://doi.org/10.1007/s10704-019-00345-1

[7] Choi Y, Ha J, Lee M-G, Korkolis YP (2021) Effect of plastic anisotropy and Portevin-Le Chatelier bands on hole-expansion in AA7075 sheets in-T6 and-W tempers. J Mater Process Technol 296:117211

[8] Zamiri A, Pourboghrat F (2007) Characterization and development of an evolutionary yield function for the superconducting niobium sheet. Int J Solids Struct 44:8627–8647. https://doi.org/https://doi.org/10.1016/j.ijsolstr.2007.06.025

[9] Lange K (1985) Handbook of metal forming. McGraw-Hill

[10] Yoon JW, Barlat F, Dick RE, Karabin ME (2006) Prediction of six or eight ears in a drawn cup based on a new anisotropic yield function. Int J Plast 22:174–193. https://doi.org/10.1016/j.ijplas.2005.03.013

[11] Moreira LP, Ferron G, Ferran G (2000) Experimental and numerical analysis of the cup drawing test for orthotropic metal sheets. J Mater Process Technol 108:78–86. https://doi.org/https://doi.org/10.1016/S0924-0136(00)00660-9

[12] Barlat F, Brem JC, Yoon JW, Chung K, Dick RE, Lege DJ, Pourboghrat F, Choi S-H, Chu E (2003) Plane stress yield function for aluminum alloy sheets—part 1: theory. Int J Plast 19:1297–1319. https://doi.org/10.1016/S0749-6419(02)00019-0

[13] Kim M, Chen K, Carriere P, Matavalam N, Penney J, Kutsaev S, Korkolis YP Mechanical Behavior and Forming of Commercially-pure Niobium Sheet. (submitted)

[14] Barlat F, Brem JC, Yoon JW, Chung K, Dick RE, Lege DJ, Pourboghrat F, Choi SH, Chu E (2003) Plane stress yield function for aluminum alloy sheets - Part 1: Theory. Int J Plast 19:1297–1319. https://doi.org/10.1016/S0749-6419(02)00019-0

[15] Logan RW, Hosford WF (1980) Upper-bound anisotropic yield locus calculations assuming {111}-pencil glide. Int J Mech Sci 22:419–430. https://doi.org/10.1016/0020-7403(80)90011-9

[16] Chen K, Scales M, Kyriakides S, Corona E (2016) Effects of anisotropy on material hardening and burst in the bulge test. Int J Solids Struct 82:70–84. https://doi.org/https://doi.org/10.1016/j.ijsolstr.2015.12.012

[17] Ha J, Baral M, Korkolis YP (2018) Plastic anisotropy and ductile fracture of bake-hardened AA6013 aluminum sheet. Int J Solids Struct 155:123–139. https://doi.org/10.1016/J.IJSOLSTR.2018.07.015

[18] Ha J, Baral M, Korkolis YP (2019) Ductile fracture of an aluminum sheet under proportional loading. J Mech Phys Solids 132:. https://doi.org/10.1016/j.jmps.2019.103685

[19] Ha J, Korkolis YP (2021) Hole-Expansion: Sensitivity of Failure Prediction on Plastic Anisotropy Modeling. J Manuf Mater Process 5:28. https://doi.org/10.3390/jmmp5020028

[20] Cullen GW, Korkolis YP (2013) Ductility of 304 stainless steel under pulsed uniaxial loading. Int J Solids Struct 50:. https://doi.org/10.1016/j.ijsolstr.2013.01.020

[21] Knysh P, Korkolis YP (2017) Identification of the post-necking hardening response of rate- and temperature-dependent metals. Int J Solids Struct 115–116:. https://doi.org/10.1016/j.ijsolstr.2017.03.012

[22] Roy BK, Korkolis YP, Arai Y, Araki W, Iijima T, Kouyama J (2022) Plastic deformation of AA6061-T6 at elevated temperatures: Experiments and modeling. Int J Mech Sci 216:106943. https://doi.org/https://doi.org/10.1016/j.ijmecsci.2021.106943

[23] Peroni L, Scapin M (2018) Experimental analysis and modelling of the strain-rate sensitivity of sheet niobium. In: EPJ Web of Conferences. EDP Sciences, p 1014